THE JOURNAL OF BIOLOGICAL CHEMISTRY VOL. 285, NO. 42, pp. 32627–32637, October 15, 2010
© 2010 by The American Society for Biochemistry and Molecular Biology, Inc. Printed in the U.S.A.

By Interacting with the C-terminal Phe of Apelin, Phe^{255} and Trp^{259} in Helix VI of the Apelin Receptor Are Critical for Internalization*[S]

Received for publication, March 25, 2010, and in revised form, July 23, 2010 Published, JBC Papers in Press, July 30, 2010, DOI 10.1074/jbc.M110.127167

Xavier Iturrioz[‡1], Romain Gerbier[‡§1,2], Vincent Leroux[¶], Rodrigo Alvear-Perez[‡], Bernard Maigret[¶], and Catherine Llorens-Cortes[‡3]

From [‡]INSERM, U691, Collège de France, Université Pierre et Marie-Curie Paris 6, Paris FR-75005, France, the [¶]Orpailleur Group, LORIA UMR CNRS 7503, H. Poincaré University, Nancy FR-54506, France, and [§]Université Paris Descarte, Paris FR-75005, France

Apelin is the endogenous ligand of the orphan seven-transmembrane domain (TM) G protein-coupled receptor APJ. Apelin is involved in the regulation of body fluid homeostasis and cardiovascular functions. We previously showed the importance of the C-terminal Phe of apelin 17 (K17F) in the hypotensive activity of this peptide. Here, we show either by deleting the Phe residue (K16P) or by substituting it by an Ala (K17A), that it plays a crucial role in apelin receptor internalization but not in apelin binding or in Gα_i-protein coupling. Then we built a homology three-dimensional model of the human apelin receptor using the cholecystokinin receptor-1 model as a template, and we subsequently docked K17F into the binding site. We visualized a hydrophobic cavity at the bottom of the binding pocket in which the C-terminal Phe of K17F was embedded by Trp^{152} in TMIV and Trp^{259} and Phe^{255} in TMVI. Using molecular modeling and site-directed mutagenesis studies, we further showed that Phe^{255} and Trp^{259} are key residues in triggering receptor internalization without playing a role in apelin binding or in Gα_i-protein coupling. These findings bring new insights into apelin receptor activation and show that Phe^{255} and Trp^{259}, by interacting with the C-terminal Phe of the pyroglutamyl form of apelin 13 (pE13F) or K17F, are crucial for apelin receptor internalization.

Apelin is a recently discovered peptide, isolated from bovine stomach extracts (1) and identified as the endogenous ligand of the human orphan G protein-coupled receptor, APJ (putative receptor protein related to the angiotensin receptor AT1) (2). Apelin is a 36-amino acid peptide derived from a single 77-amino acid precursor, preproapelin (1, 3, 4). The alignment of preproapelin amino acid sequences from cattle, humans, rats, and mice demonstrates a fully conserved C-terminal 17-amino acid sequence, apelin 17 (Lys-Phe-Arg-Arg-Gln-Arg-Pro-Arg-Leu-Ser-His-Lys-Gly-Pro-Met-Pro-Phe, K17F), including apelin 13 (Gln-Arg-Pro-Arg-Leu-Ser-His-Lys-Gly-Pro-Met-Pro-Phe). The N-terminal glutamine residue of apelin 13 may be pyroglutamylated, producing the pyroglutamyl form of apelin 13 (pE13F) (1, 3, 4). Both peptides (K17F and pE13F) are present in rat brain and plasma (5), and apelin 36 is present in testis, uterus, and bovine colostrum (3, 6). All of these peptides exhibit a high affinity for the human and the rat apelin receptors (3, 7, 8). K17F and pE13F inhibit forskolin-induced cAMP production in cells expressing either the human (3, 7) or the rat apelin receptor (9). Both peptides promote phosphorylation of ERKs, Akt, and p70 S6 kinase (10) and are highly potent inducers of apelin receptor internalization in a clathrin-dependent manner (7, 11–13).

Apelin and its receptor are both widely distributed in the brain (4, 9, 14, 15) but are particularly abundant in the hypothalamus, in the supraoptic nucleus and paraventricular nucleus, where they co-localize with arginine vasopressin (AVP)[4] in magnocellular neurons (5, 16, 17). Central injection of K17F in lactating rats inhibits the phasic firing activity of AVP neurons, thereby decreasing AVP release into the bloodstream, leading to aqueous diuresis (5). Moreover, after water deprivation, endogenous levels of AVP and apelin are conversely regulated to optimize systemic AVP release and prevent additional water loss at the kidney level (5, 17). Recently, we have also shown that such opposite regulation of plasma apelin and AVP levels by osmotic stimuli exists in humans, suggesting that apelin, like AVP, may participate in the maintenance of body fluid homeostasis in humans as in rodents (18).

Apelin and its receptor are also present in the cardiovascular system (19). Intravenous injection of apelin in rodents decreases arterial blood pressure (4, 11, 12, 20), via nitric oxide (NO) production (20). Consistent with these data, apelin causes NO-dependent arterial vasodilatation *in vivo* in humans (21), and apelin receptor-deficient mice display an exaggerated pressor response to systemic angiotensin II (AngII) (22). The hypotensive activity of apelin peptides pE13F and K17F is strictly dependent on the presence of the Phe at the C-terminal part of the apelin sequence. Thus, its deletion in K17F (K16P) (11) or its replacement by an alanine (pE13A) (23) leads to a complete loss of the hypotensive activity of these peptides.

* This work was supported by the Agence Nationale pour la Recherche "Physique et Chimie du Vivant 2009."

[S] The on-line version of this article (available at http://www.jbc.org) contains supplemental Figs. S1 and S2.

[1] Both authors contributed equally to this work.

[2] Supported by a grant "Cardiovasculaires-Obésité-Diabète" from Région Ile-de-France.

[3] To whom correspondence should be addressed: INSERM U691, Collège de France, 11 Place Marcelin Berthelot, 75231 Paris Cedex 05, France. Tel.: 33-44-27-16-63; Fax: 33-44-27-16-67; E-mail: c.llorens-cortes@college-de-france.fr.

[4] The abbreviations used are: AVP, arginine-vasopressin; MD, molecular dynamics; *M/I*, membrane/intracellular fluorescence ratio; AngII, angiotensin II; Nle, norleucine.

Finally, apelin improves cardiac contractility and reduces cardiac loading (24–26), suggesting a role for apelin in preventing heart failure. In support of this hypothesis, when apelin-deficient mice were subjected to chronic pressure overload by surgical constriction of the aorta, they developed severe and progressive heart failure (27).

Given the broad array of physiological actions of apelin, its receptor represents a new interesting target for therapeutic research and drug design. In order to design agonists or antagonists of the apelin receptor, it is important to perform structure-activity studies of apelin and to define the structural elements of the apelin receptor required for apelin binding and subsequent receptor activation. We first pharmacologically characterized the role of the C-terminal Phe of K17F. We then built a three-dimensional model of the human apelin receptor complexed with K17F and visualized a hydrophobic pocket in which the C-terminal Phe of K17F was embedded. The role of the residues constituting this pocket (Trp^{152}, Phe^{255}, and Trp^{259}) were evaluated by structure-function studies using molecular modeling and site-directed mutagenesis.

EXPERIMENTAL PROCEDURES

Drugs and Antibodies

K17F, K17A, K16P (see Table 1 for the sequences), and pE13F were synthesized by PolyPeptide Laboratories (Strasbourg, France). [^{125}I-Nle^{11},Tyr^{13}]pE13F and ^{125}I-pE13F were purchased from PerkinElmer Life Sciences and GE Healthcare, respectively. Human apelin receptor membranes from CHO cells were purchased from PerkinElmer Life Sciences.

Modeling of the Apelin-Apelin Receptor Complexes

We started first by building a homology model of the human apelin receptor itself, using for that our previous model of the cholecystokinin receptor-1 as a template (28). This model was chosen instead of the recently published x-ray structures of the β2-adrenergic and human adenosine A_{2A} receptor because (i) we are here concerned with agonists (as for the CCK1 receptor) and consequently with the "activated" conformation of the receptor and (ii) this CCK "activated" receptor model has been validated from both experiments and simulations (29, 30). Each receptor point mutation experimentally investigated in this paper was considered for MD simulations, starting from models that were obtained from the wild-type model and modified according to the mutation plug-in proposed in VMD (31).

Concerning the K17F and pE13F ligands themselves, individual models of both peptides were first built as extended peptide chains, and each one was placed in 80-Å cubic boxes of TIP3P water molecules (around 50,000 atoms in both systems). After energy refinement and MD equilibration, the conformational possibilities of these two peptides were explored by extensive 20-ns MD simulations recording a conformer snapshot each ps. The NAMD program (32) has been used for all of those simulations. Next, the conformers stored during the simulations were clustered into families presenting the same conformational behavior. Among these families, conformers presenting geometrical properties in accordance with the ones of the receptor pocket cavity were retained for building the preliminary models of ligand-receptor complexes. The MSSH (33) and SHEF (34) programs were used to compare the peptide and receptor cavity surfaces.

Finally, the receptor-ligand complexes were embedded within a palmitoyloleyl-*sn*-phosphatidylcholine bilayer placed itself within an explicit water surrounding. These models were next refined by energy minimization and submitted to MD simulations using the protocol described previously (35).

Site-directed Mutagenesis of Apelin Receptor

The cDNA-encoding rat apelin receptor cloned into pEGFP-N1 (Clontech) was used as a template to generate mutants by PCR-based site-directed mutagenesis. A first PCR was performed to generate a megaprimer that was used in a second set of PCR to generate the full-length sequence. The primer pairs (A + B) used for the first PCR were as follows: for mutant W152A and W152F, A (5′-CGCAAATGGGCGGTAGGCGTG-3′) and B (5′-CAGCCAGCACCGCCAAGACTGCTG-3′ for W152A or 5′-CAGCCAGCACGAACAAGACTGCTG-3′ for W152F); for mutant F255A and F255W, A (5′-TGCCGATTTCGGCCTATTGGTT-3′) and B (5′-GCTGGTGGTGACCGCTGCCCTGTGCTG-3′ for F255A or 5′-GCTGGTGGTGACCTGGGCCCTGTGCTG-3′ for F255W); for mutant W259A and W259F, A (5′-TGCCGATTTCGGCCTATTGGTT-3′) and B (5′-CTTTGCCCTGTGCGCGATGCCTTACC-3′ for W259A or 5′-CTTTGCCCTGTGCTTCATGCCTTACC-3′ for W259F).

The underlined bases encode the new amino acid residue replacing the naturally occurring codon. The PCR products obtained were then used as megaprimers for a second PCR with the reverse primer 5′-TGCCGATTTCGGCCTATTGGTT-3′ for mutants of Trp^{152}, and the forward primer 5′-CGCAAATGGGCGGTAGGCGTG-3′ for mutants of Phe^{255} and Trp^{259}.

The final PCR product of 2313 bp was digested with HindIII and BamHI (New England Biolabs), and the resulting 1134-bp HindIII-BamHI fragment containing the mutation was inserted into the corresponding non-mutated region (HindIII-BamHI) of the full-length apelin receptor-EGFP cDNA. Sequences of all constructs were checked by sequencing.

Transfection and Establishment of Stable Cell Line

CHO-K1 (American Type Culture Collection, Manassas, VA) cells were maintained in Ham's F-12 medium supplemented with 7% fetal calf serum, 0.5 mM glutamine, 100 units/ml penicillin, and 100 μg/ml streptomycin (all from Invitrogen). Cells were transfected with plasmid coding for wild-type and mutated apelin receptor-EGFP, using Lipofectamine 2000 (Invitrogen), and stable cell lines were established as described previously (36).

Membrane Preparations and Radioligand Binding Experiments

Crude membrane preparation from CHO stably expressing the wild-type and mutated rat apelin receptor-EGFP were prepared as described previously (37). Human apelin receptor membrane preparation was purchased from PerkinElmer Life Sciences. Membrane preparations (0.5–300 μg of total mass of membrane proteins/assay) were incubated for 60 min at 20 °C with 2×10^{-10} M ^{125}I-pE13F (GE

TABLE 1

Amino acid sequences and activity of apelin peptides in radioligand binding and cAMP production

Data represent means ± S.E. (*n*), with *n* representing the number of independent experiments performed in duplicate.

Apelin peptides	Amino acid sequences	Binding affinity (K_i)		Inhibition of forskolin-induced cAMP production (IC_{50}); rat apelin receptor-EGFP
		Rat apelin receptor-EGFP	Human apelin receptor	
		nM		*nM*
K17F	H-KFRRQRPRLSHKGPMPF-OH	0.13 ± 0.05 (7)	0.043 ± 0.02 (4)	0.16 ± 0.11 (5)
K17A	H-KFRRQRPRLSHKGPMPA-OH	0.48 ± 0.21[a] (5)	0.39 ± 0.07[b] (3)	0.7 ± 0.14[b] (6)
K16P	H-KFRRQRPRLSHKGPMP-OH	0.17 ± 0.1[c] (3)	0.061 ± 0.001[c] (3)	0.42 ± 0.1[d] (5)

[a] $p < 0.01$ compared with K17F treatment.
[b] $p < 0.001$ compared with K17F treatment.
[c] Not significantly different from K17F treatment.
[d] $p < 0.05$ compared with K17F treatment.

Healthcare) or ^{125}I-[Nle^{11},Tyr^{13}]pE13F (PerkinElmer Life Sciences) in binding buffer alone or in the presence of K17F, K16P, or K17A at various concentrations. The reaction was stopped and filtered on Whatman GF/C filters. After washing, radioactivity was counted. Saturation-binding curves were obtained by incubating membrane proteins with the radioligand at different concentrations.

cAMP Assay

The cAMP assay was performed as described previously with CHO cells stably expressing wild-type, F255A, W259A, and W259F rat apelin receptor-EGFP (9) (see Ref. 35 for details).

Internalization Assays

Confocal Microscopy—CHO cells stably expressing wild-type, F255A, W259A, and W259F rat apelin receptor-EGFP were seeded at 20% confluence on glass coverslips coated with polylysine (weight/volume 0.01%) (Sigma-Aldrich) for 30 min or 16 h for internalization experiments with K17F or lissamine-apelin 13 (see Ref. 35 for synthesis), respectively. Cells were then incubated for 90 min with 3×10^{-4} M cycloheximide. Internalization was performed by incubating the cells at 37 °C for 20 min with 10^{-6} to 10^{-11} M of K17F or lissamine-apelin 13 at 10^{-6} M as described previously (11). Cells were then mounted in Aquapolymount (Polysciences) for confocal microscopic analysis (see Ref. 35 for details). Quantification of the internalization was performed as described previously (36).

Radioligand Binding—The cells were harvested with Versene (Invitrogen). Cells (2×10^6 cells/tube for wild-type and 4×10^6 cells/tube for untransfected and mutant expressing cells) were incubated with 0.4 nM ^{125}I-pE13F in binding buffer (50 mM Hepes, pH 7.4, 5 mM $MgCl_2$, 1% BSA, and 0.1% glucose) for 2 h at 4 °C. The cells were washed twice with ice-cold binding buffer and resuspended in 200 μl of binding buffer. Cells were then incubated at 37 °C for 0 and 20 min and centrifuged at 500 × g. Cell pellets were washed with 500 μl of acid buffer (0.5 M NaCl, 0.2 M acetic acid, pH 2) for 15 min at 4 °C and centrifuged. Pellets (intracellular fractions) were resuspended in 500 μl of acid buffer, and radioactivity was counted.

Data Analysis

Binding experiment and cAMP experiment data were analyzed with GraphPad Prism. Statistical comparisons were performed with Student's unpaired *t* test or with one-way analysis of variance with Dunnet's post-test using GraphPad Prism. Differences were considered significant when *p* was <0.05.

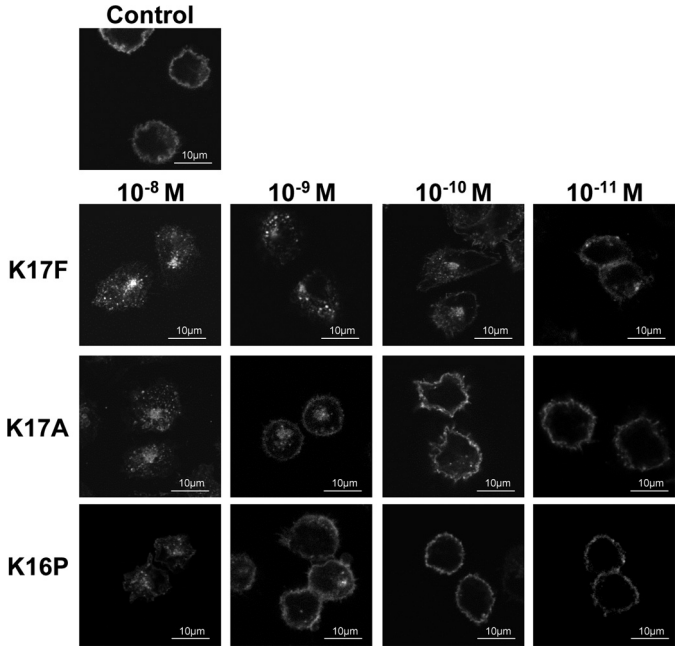

FIGURE 1. **Internalization of the rat apelin receptor-EGFP by different apelin K17F fragments.** CHO cells stably expressing the rat apelin receptor-EGFP were stimulated with 10^{-8}, 10^{-9}, 10^{-10}, and 10^{-11} M K17F, K17A, and K16P. After 20 min of stimulation, cells were fixed and analyzed by confocal microscopy. Each *panel* is representative of three separate experiments.

RESULTS

Role of the C-terminal Phenylalanine of Apelin in Radioligand Binding, cAMP Production, and Apelin Receptor Internalization

We first investigated the role of the C-terminal Phe of K17F (Table 1) by deleting (K16P) or substituting this residue by an Ala (K17A) (see Table 1 for sequences). We then analyzed the *in vitro* pharmacological profile of these peptides by determining their binding properties and their ability to inhibit forskolin-induced cAMP production and to trigger apelin receptor internalization (Table 1 and Fig. 1).

Radioligand Binding—We first determined, by performing saturation curves, the apparent dissociation constants (K_d) for the human apelin receptor and the rat apelin receptor tagged at its C-terminal part with EGFP (apelin receptor-EGFP) stably expressed in CHO cells using ^{125}I-pE13F as radioligand, and they were 1 and 0.65 nM, respectively.

The K_i values of K17F for the human apelin receptor and the rat apelin receptor-EGFP were 0.04 ± 0.02 nM ($n = 4$) and 0.13 ± 0.05 nM ($n = 7$), respectively. Deletion of the C-terminal

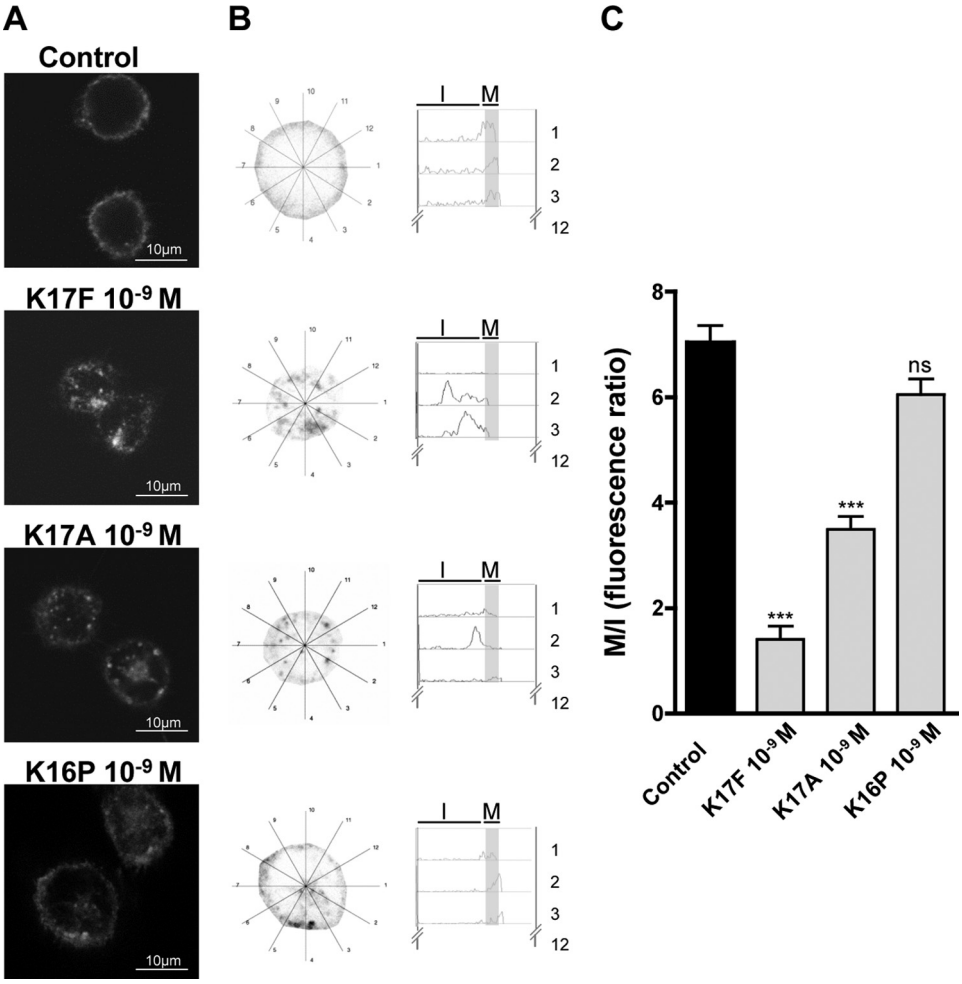

FIGURE 2. **Quantification of rat apelin receptor-EGFP internalization.** *A*, confocal images of CHO cells stably expressing the rat apelin receptor-EGFP incubated without (*Control*) or with K17F, K17A, and K16P at 10^{-9} M for 20 min. *B*, example of *gray scale* conversion and median filtering of a cell with 12 radial measurement lines *outlined*. Shown are example plots of *gray scale* density distribution along the first three radial measurement lines for a cell. The mean density value of the first 30 pixels (*shaded*), represents the plasma membrane and leads to the *M* value, and the mean density of the remaining intracellular pixels leads to the *I* value. The mean of the 12 *M* values and the 12 *I* values is used to calculate the *M*/*I* ratio for each cell. *C*, histogram of *M*/*I* ratios. The results are expressed as means ± S.E. (*error bars*) ($n = 5$). Statistical differences were assessed using one-way analysis of variance with Dunnet's post-test. *n.s.*, not significantly different from control; ***, $p < 0.001$.

Phe of K17F (K16P) did not modify the K_i values for the human or rat apelin receptors as compared with K17F, and they were 0.06 ± 0.001 nM ($n = 3$) and 0.17 ± 0.1 nM ($n = 3$), respectively, whereas the K_i of K17A was slightly but significantly modified and was 0.39 ± 0.07 nM ($n = 3$) for the human apelin receptor and 0.48 ± 0.21 nM ($n = 5$) for the rat apelin receptor-EGFP. Interestingly, the change in the affinity of K17A for the rat apelin receptor (by a factor of 3.5) is less marked than that observed for the human apelin receptor (by a factor of 10), showing a small difference in the mode of binding of the apelin receptor in rats and humans.

cAMP Production—Incubation of CHO cells stably expressing the rat apelin receptor-EGFP with increasing concentrations (10^{-13} to 10^{-6} M) of K17F, K17A, or K16P resulted in a concentration-dependent inhibition of forskolin-induced cAMP production with IC_{50} of 0.16 ± 0.11 nM ($n = 5$), 0.7 ± 0.14 nM ($n = 6$), and 0.42 ± 0.1 nM ($n = 5$), respectively (Table 1). The maximal inhibitory effects of K17F (94%), K16P (86%), and K17A (91%) on forskolin-induced cAMP production occurred for concentrations equal to or greater than 10 nM.

Apelin Receptor-EGFP Internalization—Confocal microscope analysis of CHO cells stably expressing the rat apelin receptor-EGFP in resting conditions displayed an intense apelin receptor-EGFP fluorescence at the plasma membrane (Fig. 1). Incubation with increasing concentrations (from 10^{-11} to 10^{-8} M) of K17F for 20 min resulted in a marked decrease of surface-associated fluorescent label and the appearance of numerous fluorescent intracytoplasmic vesicles (Fig. 1). Incubation with increasing concentrations (from 10^{-11} to 10^{-8} M) of K16P or K17A for 20 min resulted in a different internalization pattern of the rat apelin receptor-EGFP, showing that both peptides are less potent than K17F. This was prominent when peptides were applied at a concentration of 10^{-9} M (Fig. 2). Indeed, the membrane/intracellular fluorescence ratios (*M*/*I*) induced by 10^{-9} M K17F (*M*/*I* = 1.4 ± 0.6, $n = 5$), 10^{-9} M K17A (*M*/*I* = 3.5 ± 0.5, $n = 5$), or 10^{-9} M K16P (*M*/*I* = 6.0 ± 0.7, $n = 5$) revealed that whereas K17F already induced a robust internalization of the apelin receptor-EGFP, a significant but modest internalization of the rat apelin receptor-EGFP was promoted by K17A, and no internalization was detected with K16P (Fig. 2). At 10^{-11} M, only K17F induced a modest internalization (see *arrows*), whereas K17A- and K16P-treated cells displayed a plasma membrane fluorescent labeling similar to that of untreated cells (control cells).

Molecular Modeling of Apelin Ligands, Human Apelin Receptor, and Ligand-Receptor Complexes

Modeling of the K17F and pE13F Peptides—From the clustering analysis of the MD trajectory of K17F and pE13F in solution (Fig. 3*A*), we have found that the whole conformational space of both peptides can be expressed as nine conformational families, which are shown in Fig. 3*B* for pE13F. The shape analysis of the most representative conformations extracted from each family has shown that only family number 9 is able to accommodate the receptor cavity. Consequently, only the representative conformation of cluster 9 was taken to build the complexes by docking the corresponding conformation inside the receptor putative binding site.

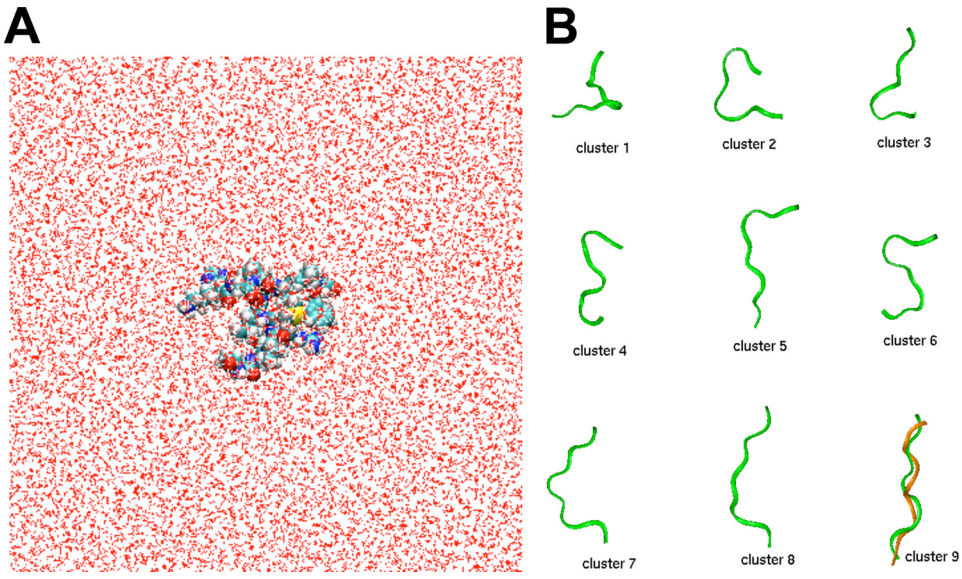

FIGURE 3. **Modeling of pE13F peptide.** *A*, pE13F peptide in a water box. *B*, typical *ribbon-like drawings* of the nine clusters representing the pE13F conformational space (in *green*). Cluster 9 typical conformations were used to dock pE13F in the apelin receptor. The conformation found in the complex with the receptor after the MD simulations is represented in *orange*.

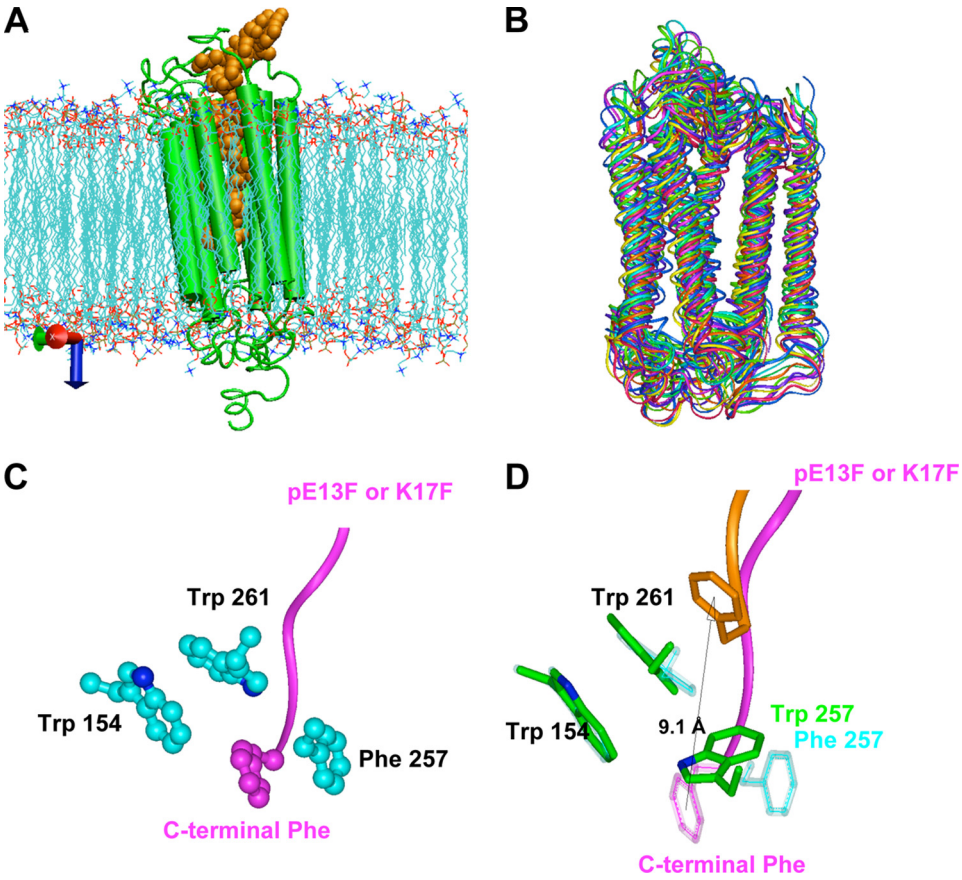

FIGURE 4. **Modeling of the wild-type and F257W mutated human receptors complexed with K17F and pE13F.** *A*, the human apelin receptor-K17F complex embedded in a bilayer membrane of palmitoyloleyl-*sn*-phosphatidylcholine surrounded by water molecules. *B*, fluctuations observed after extensive MD simulations of the apelin receptor-K17F complex. *C*, detailed view of the aromatic cavity where C-terminal Phe of pE13F or K17F are embedded. The peptide is indicated in *pink*, whereas the apelin receptor residues are indicated in *blue*. *D*, overlapping of the detailed views of the aromatic pocket in the wild-type human receptor (*transparent blue*) and in the F257W mutated receptor (*green*) showing the changes in the binding of the C-terminal Phe of pE13F or K17F (in *pink* for the wild-type receptor and in *orange* for the F257W mutated receptor). The *arrow* indicates the displacement of the C-terminal Phe by 9.1 Å.

Modeling the Wild-type Receptor-K17F and -pE13F Complexes—After the minimization and MD equilibration steps, it appears from the analysis of the recorded MD trajectory that the models of the receptor-K17F (Fig. 4*A*) and receptor-pE13F (data not shown) complexes are stable, presenting only weak fluctuations, at least as concerns the transmembrane helices (Fig. 4*B*). A detailed analysis of the intermolecular peptide-receptor interactions shows that the peptide is anchored within the binding receptor cavity mainly through strong electrostatic interactions at the entry of the receptor binding site and π-π stacking at the bottom of the cavity (Fig. 4*C*). These last interactions involve the C-terminal Phe of K17F and pE13F and an aromatic pocket formed by the aromatic side chains of Trp^{154} in TMIV and of Phe^{257} and Trp^{261} in TMVI in the human apelin receptor. These residues correspond to Trp^{152}, Phe^{255}, and Trp^{259} in the rat apelin receptor (Fig. 4*C* and supplemental Fig. S2).

Modeling of the Mutated Complexes—We performed the MD simulations concerning the receptor aromatic pocket residues using the same protocol as above. It appears from these simulations that, at least during the present simulated time (20 ns), few changes occur except for the F257W mutant. In this case, the K17F peptide moved up away from the binding pocket, due to a change of the Trp^{257} residue moving toward the indole side chain of Trp^{261} and Trp^{154} and therefore closing the aromatic pocket (Fig. 4*D*).

Site-directed Mutagenesis and Expression of Recombinant Wild-type and Mutated Apelin Receptor-EGFP

In order to validate the three-dimensional model of the human apelin receptor complexed with pE13F and K17F, we substituted by site-directed mutagenesis the residues Trp^{152} and Trp^{259} either by an Ala (W152A and W259A) or

TABLE 2

Binding parameters of wild-type and mutated rat apelin receptors for [^{125}I-Nle^{11},Tyr^{13}]pE13F

K_d and B_{max} values were obtained from saturation experiments using [^{125}I-Nle^{11},Tyr^{13}]pE13F as radioligand on crude membrane preparations from CHO cells stably expressing wild-type and mutated rat apelin receptor-EGFP. Data represent the means ± S.E. obtained from *n* independent experiments performed in duplicate. ND, not determined.

Apelin receptor-EGFP	K_d	B_{max}
	nM	*fmol/mg*
Wild type	0.95 ± 0.26 ($n = 3$)	48 ± 3.8 ($n = 3$)
W152A	ND	ND
F255A	0.73 ± 0.19[a] ($n = 4$)	10 ± 3.2[b] ($n = 4$)
F255W	ND	ND
W259A	0.27 ± 0.06[b] ($n = 3$)	2 ± 0.6[b] ($n = 3$)
W259F	0.44 ± 0.03[c] ($n = 3$)	2 ± 1.3[b] ($n = 3$)

[a] Not significantly different from wild-type receptor.
[b] $p < 0.01$ compared with wild-type receptor.
[c] $p < 0.05$ compared with wild-type receptor.

a Phe (W152F and W259F) and Phe^{255} by an Ala (F255A) or a Trp (F255W). Constructs encoding wild-type and mutated apelin receptor-EGFP were transfected and stably expressed in CHO cells. We first verified that the mutations did not affect the production and processing of the recombinant proteins by investigating the subcellular distribution of wild-type and mutated apelin receptor-EGFP in stably transfected CHO cells by confocal microscopy analysis (supplemental Fig. S1). Thus, we showed that the recombinant wild-type F255A and F255W apelin receptors were similarly located at the plasma membrane (supplemental Fig. S1 and Fig. 7*A*), whereas W259A and W259F mutants were partially expressed at the plasma membrane but remained mainly trapped in an intracellular network possibly corresponding to the endoplasmic reticulum (supplemental Fig. S1 and Fig. 8*A*). The W152A mutant displayed an intracellular expression, whereas we did not detect any expression for the W152F mutant (several cell lines were analyzed; data not shown), probably reflecting a misfolding of the apelin receptor associated with the mutation of the Trp^{152} residue. We therefore did not carry out the pharmacological characterization of the W152F mutant.

Binding Properties of Wild-type and Mutated Rat Apelin Receptor-EGFP

We then characterized the binding properties of wild-type and mutated apelin receptors. We first determined, by performing saturation curves, the apparent dissociation constant (K_d) and the maximal receptor density (B_{max}) values for recombinant wild-type and mutated (W152A, F255A, F255W, W259A, W259F) apelin receptors using [^{125}I-Nle^{11},Tyr^{13}]pE13F as a radioligand (Table 2). The K_d values were 0.95 ± 0.26 nM ($n = 3$) for the wild-type rat apelin receptor-EGFP and 0.73 ± 0.19 nM ($n = 4$), 0.27 ± 0.06 nM ($n = 3$), and 0.44 ± 0.03 nM ($n = 3$) for the F255A, W259A, and W259F mutants, respectively, whereas no binding was observed with W152A and F255W mutated apelin receptors (Table 2). Although the K_d values of the mutated apelin receptors were close to the K_d value of the wild-type apelin receptor, the B_{max} values of the mutated receptors were strongly decreased as compared with wild-type apelin receptor and were 48 ± 3.8 fmol/mg total protein ($n = 3$), 10 ± 3.2 fmol/mg ($n = 4$), 2 ± 0.6 fmol/mg ($n = 3$), and 2 ± 1.3 fmol/mg ($n = 3$) for the wild-type and F255A, W259A, and W259F mutated apelin receptors, respectively (Table 2). Furthermore, K17F dose-dependently inhibited specific binding to the wild-type, F255A, W259A, and W259F apelin receptors with K_i values of 0.32 ± 0.08 nM ($n = 9$), 0.19 ± 0.05 nM ($n = 7$), 0.06 ± 0.01 nM ($n = 4$), and 0.11 ± 0.07 nM ($n = 4$), respectively (Fig. 5 and Table 3).

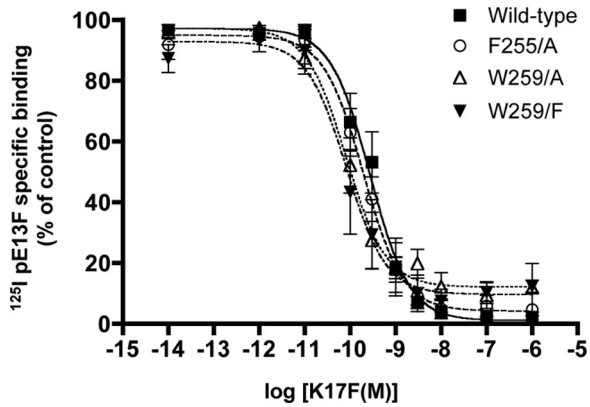

FIGURE 5. **Binding potency of K17F on the wild-type and mutated rat apelin receptor-EGFP.** Competitive binding activity of K17F with membranes from CHO cells stably expressing the rat apelin receptor. Membranes of CHO cells stably expressing the rat apelin receptor were incubated with 2 × 10^{-10} M [^{125}I-Nle^{11},Tyr^{13}]pE13F in the presence of increasing concentrations of K17F (from 10^{-6} to 10^{-14} M). Data are expressed as percentage of maximal binding of [^{125}I-Nle^{11},Tyr^{13}]pE13F in the absence of any nonradiolabeled ligand and represent the mean ± S.E. (*error bars*) of 4–9 independent experiments performed in duplicate.

TABLE 3

Inhibition constants (K_i) of K17F for the wild-type and mutated rat apelin receptors

K_i values were determined by competition binding assays performed by displacement of [^{125}I-Nle^{11},Tyr^{13}]pE13F. Data represent the means ± S.E. obtained from *n* independent experiments performed in duplicate.

Apelin receptor-EGFP	K_i	*n*
	nM	
Wild type	0.32 ± 0.08	9
F255A	0.19 ± 0.05[a]	7
W259A	0.06 ± 0.01[a]	4
W259F	0.11 ± 0.07[a]	4

[a] $p < 0.01$ significantly different from wild type.

Inhibition of Forskolin-induced cAMP Production by Wild-type and Mutated Apelin Receptor-EGFP

Incubation of CHO cells stably expressing the wild-type rat apelin receptor-EGFP or the F255A, W259A, and W259F mutants with increasing concentrations of K17F (10^{-14} to 10^{-6} M) resulted in a concentration-dependent inhibition of forskolin-induced cAMP production (Fig. 6) with an IC_{50} value of 0.12 ± 0.04 nM ($n = 13$), 0.48 ± 0.19 nM ($n = 7$), 0.10 ± 0.02 nM ($n = 5$), and 0.21 ± 0.12 nM ($n = 4$), respectively (Table 4). No detectable inhibition of cAMP production was observed in untransfected CHO cells treated with 10 μM forskolin (data not shown). The maximal inhibitory effects of K17F (between 66 and 86%) on forskolin-induced cAMP production in CHO cells stably expressing the wild-type or mutated apelin receptors occurred for concentrations equal to or greater than 10^{-8} M (Fig. 6).

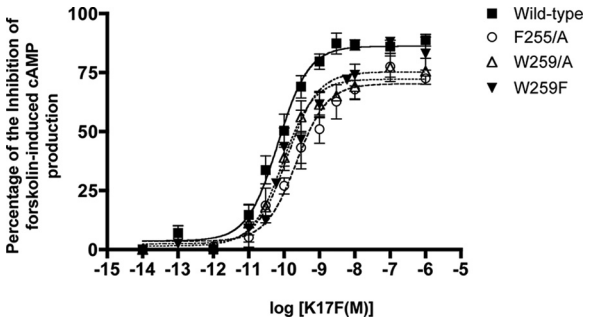

FIGURE 6. **Effect of K17F on forskolin-induced cAMP production in CHO cells stably expressing the wild-type and mutated rat apelin receptor-EGFP.** cAMP production was induced by treatment of cells with 10^{-5} M forskolin in CHO cells stably expressing wild-type, F255A, W259A, and W259F rat apelin receptor-EGFP. Effects of various concentrations of K17F from 10^{-6} to 10^{-14} M on forskolin-induced cAMP production were then evaluated. Each point represents the mean ± S.E. (*error bars*) of 4–13 independent experiments performed in duplicate.

TABLE 4

Effects of apelin receptor mutations on K17F-induced inhibition of cAMP production

The effect of K17F was examined at concentrations from 10^{-13} to 10^{-7} M in the presence of 10^{-5} M forskolin on CHO cells stably expressing the wild-type or mutated rat apelin receptor-EGFP. The IC_{50} values were obtained by analyzing the dose-response curves of cAMP production with a non-linear equation (GraphPad Prism). Data represent the means ± S.E. obtained from *n* independent experiments performed in duplicate.

Apelin receptor-EGFP	IC_{50}	*n*
	nM	
Wild type	0.12 ± 0.04	13
F255A	0.48 ± 0.19[a]	7
W259A	0.10 ± 0.02[b.]	5
W259F	0.21 ± 0.12[b]	4

[a] $p < 0.01$ compared with wild-type receptor.
[b] Not significantly different from wild-type receptor.

Internalization of Wild-type and Mutated Apelin Receptor-EGFP

We finally evaluated the effect of the mutations on the capacity of the mutated apelin receptors to internalize following K17F (Fig. 7*A*) or lissamine-apelin 13 application (Fig. 8*A*). Because recombinant apelin receptors were tagged at their C-terminal part with EGFP, we could visualize apelin receptor internalization by following the redistribution of the fluorescence from the plasma membrane compartment to small cytoplasmic fluorescent vesicles (Fig. 7*A*). Incubation of wild-type apelin receptor-EGFP stably transfected CHO cells with 10 nM or 1 μM K17F for 20 min, resulting in a marked endocytosis of the apelin receptor as shown by the disappearance of fluorescence at the plasma membrane and the appearance of numerous intracellular fluorescent vesicles, leading to a switch of the *M*/*I* ratio from 7.1 ± 0.9 ($n = 5$) to 0.09 ± 0.2 ($n = 5$) (Fig. 7, *A* and *B*). In contrast, incubation of F255A stably transfected CHO cells with 10 nM or 1 μM K17F for 20 min displayed an intense apelin receptor-EGFP fluorescence at the level of the plasma membrane without intracellular fluorescent vesicles, and no difference in the *M*/*I* ratio was observed between control cells (3.6 ± 0.8, $n = 5$) and cells treated with 1 μM K17F (3.5 ± 0.5, $n = 5$) (Fig. 7*B*). As expected, CHO cells stably expressing the F255W mutant, which did not bind [^{125}I-Nle^{11},Tyr^{13}]apelin 13, did not exhibit a profile of internalization (Fig. 7, *A* and *B*). Because

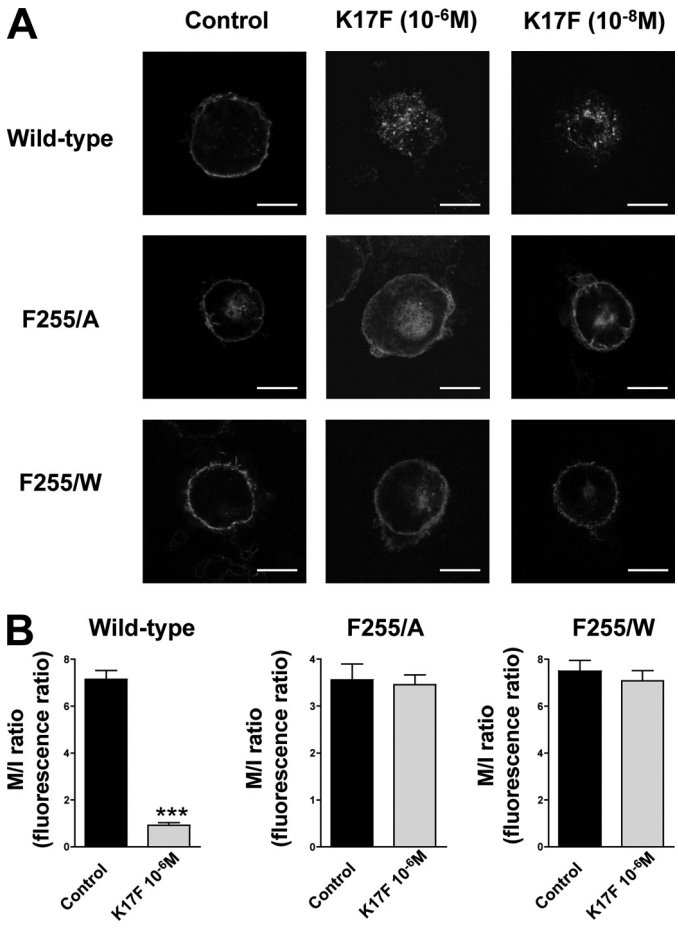

FIGURE 7. **Internalization of the wild-type, F255A, or F255W rat apelin receptor-EGFP by K17F.** *A*, CHO cells stably expressing wild-type, F255A, and F255W rat apelin receptor-EGFP were stimulated for 20 min without (*Control*) or with 10^{-6} or 10^{-7} M K17F. Cells were then fixed and analyzed by confocal microscopy. Each *panel* is representative of at least three independent experiments. *B*, quantification of wild-type, F255A, and F255W rat apelin receptor-EGFP internalization induced by 10^{-6} M K17F. *M*/*I* ratios are expressed as means ± S.E. (*error bars*) of five independent experiments. Statistical differences were assessed using Student's *t* test. *n.s.*, not significantly different from control; ***, $p < 0.001$. *Scale bars*, 10 μm.

W259A and W259F cell lines displayed strong intracellular apelin receptor-EGFP fluorescence, it was impossible to visualize directly the endocytosis of the receptor by following EGFP fluorescence. Alternatively, we followed the endocytosis of a fluorescent apelin fragment, lissamine-apelin 13 (Fig. 8*A*). Treatment of wild-type apelin receptor cell line with 1 μM lissamine-apelin 13 induced a strong endocytosis of the fluorescent ligand (*red*) that perfectly overlapped with the fluorescence of apelin receptor-EGFP (*green*) within vesicular structures (Fig. 8*A*). Interestingly, although the W259A cell line did not display any intracellular lissamine-apelin 13-containing vesicles, the W259F cell line displayed a few lissamine-apelin 13-containing vesicles, indicated by *arrowheads* (Fig. 8*A*). In order to confirm these results, we quantified internalization by monitoring internalization of radiolabeled apelin (Fig. 8*B*). According to confocal analysis, only wild-type and W259F apelin receptors expressing cells showed an increase in radioactivity in the intracellular fraction after 20 min of incubation at 37 °C (Fig. 8*B*).

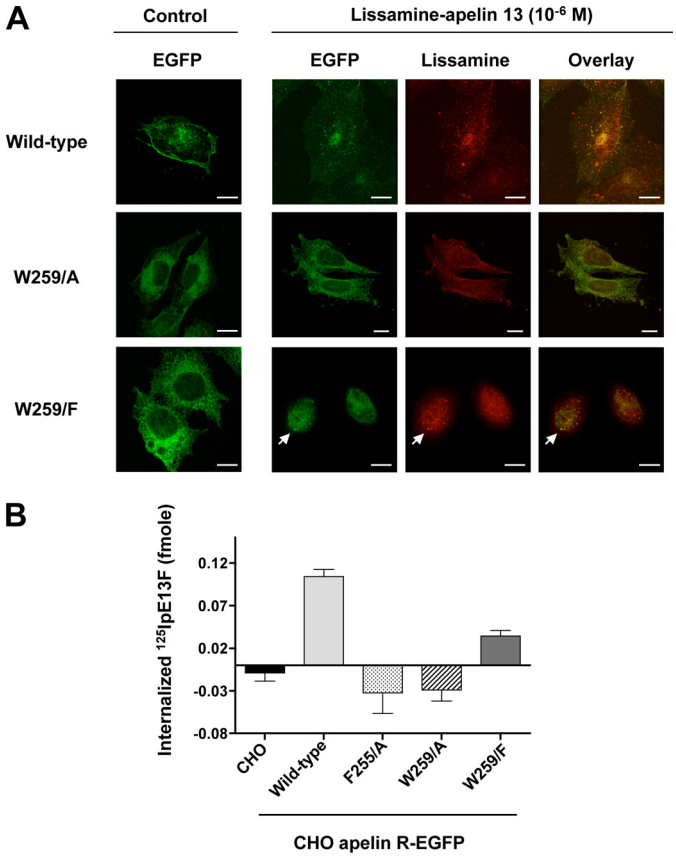

FIGURE 8. **Internalization of the wild-type and mutated rat apelin receptor-EGFP by lissamine-apelin 13 or ^{125}I-pE13F.** *A*, CHO cells stably expressing wild-type, W259A, and W259F rat apelin receptor-EGFP were stimulated for 20 min without (*Control*) or with 10^{-6} M of lissamine-apelin 13. Cells were then fixed and analyzed by confocal microscopy. Fluorescence corresponding to rat apelin receptor-EGFP was visualized in *green*, and fluorescence corresponding to lissamine-apelin 13 was visualized in *red*. The overlay was visualized in *yellow*, and the *arrowheads* showed vesicular structures. Each panel is representative of at least three independent experiments. *B*, internalization of ^{125}I-pE13F with untransfected CHO cells (CHO K1) or CHO cells stably expressing wild-type, F255A, W259A, and W259F rat apelin receptor-EGFP. Cells were incubated with ^{125}I-pE13F (4×10^{-10} M) for 2 h at 4 °C and then washed with ice-cold buffer and incubated at 37 °C for 20 min in binding buffer. The extent of internalization was then determined by comparing the amount of radioactivity (in fmol) present inside the cells between time 0 min and time 20 min. The *histogram* is representative of three independent experiments. *Scale bars*, 10 μm. *Error bars*, S.D.

DISCUSSION

In the present work, we showed that the C-terminal Phe of apelin plays a critical role in apelin receptor internalization but was not involved in apelin binding or in $G\alpha_i$ coupling. We built a three-dimensional model of the apelin receptor complexed with K17F or pE13F, showing that the Arg in position 6 and 2 in K17F and pE13F, respectively, interacted with acidic residues at the top of the receptor and that the C-terminal Phe of both apelin peptides was embedded into an hydrophobic pocket composed of three main aromatic residues: Trp^{152} in TMIV and Phe^{255} and Trp^{259} in TMVI of the rat apelin receptor. Using molecular modeling and site-directed mutagenesis studies, we demonstrated that the residues Phe^{255} and Trp^{259} in the apelin receptor by interacting with the C-terminal Phe of pE13F are crucial for apelin receptor internalization.

Alascan and deletion studies of the apelin peptides, pE13F and K17F, showed that the Arg and Leu residues at positions 2 and 5 in pE13F and positions 6 and 10 in K17F are crucial for apelin binding (7, 11). In contrast, the Ala substitution of the C-terminal Phe in pE13F (pE13A) did not affect its capacity to bind to the apelin receptor (7). Moreover, the deletion of the C-terminal Phe in K17F (K16P) did not modify its ability to inhibit forskolin-induced cAMP production (11). However, when pE13A and K16P are injected intravenously in rats, they lose their capacity to decrease arterial blood pressure when compared with the corresponding natural peptides pE13F and K17F (11, 23). To understand how the C-terminal Phe of K17F activates the apelin receptor, we first characterized the pharmacological properties of K17F, K17A, and K16P related to the apelin receptor (binding, cAMP production, and internalization). The deletion or the substitution of the C-terminal Phe of K17F by an Ala did not strongly modify the affinity of K16P or K17A for the apelin receptor and very slightly affected their capacity to inhibit cAMP production, effects similar to those reported for pE13A (7). These data indicate that the C-terminal Phe of K17F did not play a major role in K17F binding to the apelin receptor or in its capacity to activate $G\alpha_i$. In contrast, the ability of these peptides (K17A and K16P) to induce the internalization of the apelin receptor is drastically reduced as compared with K17F, and the effect was even more marked with K16P *versus* K17A, pointing out the crucial role played by the C-terminal Phe of K17F to trigger apelin receptor internalization. Considering the lack of blood pressure decrease induced by K16P and pE13A compared with K17F (11, 23), this suggests that the hypotensive activity of K17F required the presence of the C-terminal Phe residue and consequently apelin receptor internalization. We can therefore hypothesize that K17F, by inducing apelin receptor internalization, subsequently provokes the activation of a second signaling pathway, $G\alpha_i$-independent but β-arrestin-dependent. This functional dissociation suggests that the apelin receptor exists in different active conformations depending on the ligand fitting into the binding site and leading to the activation of different signaling pathways. This is in line with the concept of biased agonists. Such agonists stabilize distinct receptor conformations that differ in their signaling partner preference that will thus induce different biological responses as shown for β-adrenergic receptors, AT1a, and parathyroid hormone receptors (38–41).

To understand how the C-terminal Phe residue of apelin interacts within the apelin receptor binding site to induce this functional dissociation, we built a three-dimensional model of the rat apelin receptor complexed with pE13F or K17F. Similar results were obtained with both peptides. Analysis of the models complexed with pE13F or K17F showed that the Arg in position 2 or 6 in pE13F or K17F interacted within the top of the receptor with acidic residues and that the C-terminal Phe of pE13F was docked into a hydrophobic pocket composed of three main residues located in the TM of the apelin receptor, Trp^{152} in TMIV and Phe^{255} and Trp^{259} in TMVI. All of these residues are highly conserved among G protein-coupled receptors (supplemental Fig. S2). Clusters of TM aromatic residues have already been identified as an important moiety for G protein-coupled receptors functioning (42–46). In such clusters, particular interest has been taken in the tryptophan (47–49) and phenylalanine (50–53) side chains found in TM helices,

which were demonstrated as key residues for ligand binding and/or receptor activation. In biological systems, π-π interactions have been established as bringing an important contribution to the stability and flexibility of molecular associations (54, 55). In the AT1 receptor, which is phylogenetically closely related to the apelin one, an aromatic cluster has also been detected involving a π-π stacking with the Phe residue of the ligand, angiotensin II (56).

To ensure the veracity of these interactions, visualized in the three-dimensional model of the apelin receptor-apelin complexes, we studied the role of Trp^{152}, Phe^{255}, and Trp^{259} by site-directed mutagenesis studies. Each residue was substituted by an Ala in order to abolish the possible interaction of the C-terminal Phe of pE13F with the side chains of these residues. Phe^{255} was also substituted by a Trp, and Trp^{152} and Trp^{259} were substituted by a Phe to conserve the aromatic property of the side chains. Conversion of Trp^{152} to Ala or Phe led to misfolded proteins that were not able to bind pE13F, suggesting that Trp^{152} is essential for apelin receptor structure integrity. This is in line with the data obtained with different G protein-coupled receptors, such as CB2 cannabinoid, M3 muscarinic, and δ-opioid receptors, in which the mutations of the equivalent residues led to a decrease in the binding of their respective ligands (42, 48, 57). However, these substitutions led to less important changes than those we observed for the apelin receptor. This suggested that Trp^{152} has probably a more critical role in maintaining the structural integrity of the apelin receptor than the corresponding Trp residues in the CB2, M3, or δ-opioid receptors.

The substitutions of Phe^{255} by an Ala or a Trp led to the expression of mutated apelin receptors correctly folded and expressed at the plasma membrane. As expected, the F255A mutated receptor kept its ability to bind apelin but with a reduction (factor of 5) in maximal receptor density, whereas the F255W mutated receptor lost its ability to bind apelin despite its correct expression at the cell surface. These data fitted with the interactions visualized in the three-dimensional model of the F255W mutated receptor complexed with pE13F that showed that the substitution of Phe by a Trp induces a reorganization of the aromatic pocket, projecting the C-terminal Phe of pE13F far beyond the hydrophobic pocket. This reorganization also modified the position of Arg^2 or Arg^6 of pE13F or K17F in the binding site, preventing it from optimally binding with the acidic residues located at the top of the receptor, as shown in the three-dimensional model of wild-type and F255A apelin receptors. Finally, the conversion of Trp^{259} to Ala or Phe led to a partial expression of receptors at the cell surface with a high intracellular expression. However, W259A and W259F mutated receptors were able to bind apelin but, as expected, with a major reduction (factor of 24) in maximal binding capacity. These data suggest that Trp^{259} plays a structural role and that its mutation induced a delay in protein maturation without totally impairing receptor folding.

The replacement of Phe^{255} by Ala or that of Trp^{259} by Ala or Phe slightly increases the affinity of apelin for these mutated receptors when compared with the wild-type apelin receptor, demonstrating that Phe^{255} and Trp^{259} are not key residues for apelin binding. Moreover, the changes induced by these mutations on the inhibitory potency of K17F on forskolin-induced cAMP production were of very small amplitude, only a 4-fold decrease for the F255A mutation and no significant change for the W259A and W259F mutations, showing that Phe^{255} and Trp^{259} are not critically involved in $G\alpha_i$-protein coupling. These results slightly contrast with those obtained with α_{1b}- and β_2-adrenergic receptors for which the residues equivalent to Phe^{255}, Phe^{303}, and Phe^{282}, respectively, were shown to be key residues for TMVI helical movements to G-protein activation (51, 58). The equivalent residue (Phe^{609}) in the oxytocin receptor has also been studied (59). Its substitution by a Tyr, the equivalent residue present in the vasopressin receptor, did not change oxytocin binding affinity and slightly reduced that of AVP. However, this mutation, which did not modify the ability of oxytocin to increase inositol phosphate production, drastically increased that of AVP, highlighting the role of this residue in the activation selectivity of the oxytocin receptor by oxytocin (59). These differences between the apelin receptor and adrenergic receptors or oxytocin receptor could be related to different modes of binding of structurally different ligands.

But the most interesting observation concerned the total inability of the mutated receptors, F255A, W259A, and F255W, to internalize upon agonist stimulation even at a supramaximal concentration of K17F and lissamine-apelin 13. However, a more conservative mutation, such as W259F, maintained the ability of the mutated receptor to internalize but with a weaker efficiency when compared with wild-type apelin receptor, in line with the lower expression of the mutated receptor at the cell surface. Altogether, our data demonstrated that Phe^{255} and, to a lesser extent, Trp^{259} are key residues for apelin receptor internalization without playing a role in binding nor in activation of G-protein coupling. Interestingly, analysis of the three-dimensional models of the CCK1 and AT1 receptors complexed with CCK8 and AngII, respectively, two peptides exhibiting a Phe at their C-terminal part, showed that the Phe residue in both peptides was located in the vicinity of a Trp residue, Trp^{236} in CCK1R and Trp^{253} in AT1R. However, the roles of these Trp residues are different from that found for Trp^{259} in the apelin receptor. Trp^{326} in CCK1R plays a role in G-protein coupling activation by interacting with C-terminal Phe of the CCK8 (60), whereas Trp^{253} in AT1R plays an indirect role in the binding of AngII by stabilizing the ionic bridge formed between the free carboxylate anion of the C-terminal Phe of AngII and the amino group of Lys^{199} of AT1 (61).

These data constitute the first experimental validation of the three-dimensional model of the apelin receptor complexed with pE13F/K17F, showing the docking of the C-terminal Phe of apelin, within an aromatic pocket of the receptor constituted by Phe^{255} and Trp^{259}. The mutation of these residues as well as the deletion or the substitution of the C-terminal Phe in apelin abolishes apelin receptor internalization. This shows the crucial role played by the C-terminal Phe of apelin, which, by interacting with these residues in the apelin receptor, induced a conformation of the receptor required for its internalization that may be responsible for the apelin-induced decrease in blood pressure. Recently, we isolated the first non-peptidic apelin receptor agonist, E339-3D6, which behaved as a partial agonist with regard to cAMP production and as a full agonist with

regard to apelin receptor internalization (35). Moreover, despite its affinity (90 nM) lower than that of K17F, E339-3D6 was as efficient as K17F in inducing rat aorta vasorelaxation (35). Interestingly, the docking of E339-3D6 into the apelin receptor three-dimensional model has shown that the lissamine moiety in this molecule fits within the aromatic pocket constituted by Phe^{255} and Trp^{259}. This could account for the full agonist character of E339-3D6 with regard to receptor internalization.

In conclusion, this work brings new insight into the mode of activation of the apelin receptor and particularly into the mechanism that triggers apelin receptor internalization and apelin-induced blood pressure decrease. Further studies are being undertaken to better understand the structural and functional organization of this receptor and to definitively validate the three-dimensional model of the apelin receptor-pE13F complex. Such a three-dimensional model would be then used to perform *in silico* screening of virtual chemical libraries or for the optimization of hits isolated from classical screenings. This will allow the design of biased agonists targeting a specific physiological response.

Acknowledgments—We thank M. Hibert and D. Bonnet for kindly providing lissamine-Apelin 13 and I. Banegas-Font for technical assistance.

REFERENCES

1. Tatemoto, K., Hosoya, M., Habata, Y., Fujii, R., Kakegawa, T., Zou, M. X., Kawamata, Y., Fukusumi, S., Hinuma, S., Kitada, C., Kurokawa, T., Onda, H., and Fujino, M. (1998) *Biochem. Biophys. Res. Commun.* **251,** 471–476
2. O'Dowd, B. F., Heiber, M., Chan, A., Heng, H. H., Tsui, L. C., Kennedy, J. L., Shi, X., Petronis, A., George, S. R., and Nguyen, T. (1993) *Gene* **136,** 355–360
3. Habata, Y., Fujii, R., Hosoya, M., Fukusumi, S., Kawamata, Y., Hinuma, S., Kitada, C., Nishizawa, N., Murosaki, S., Kurokawa, T., Onda, H., Tatemoto, K., and Fujino, M. (1999) *Biochim. Biophys. Acta* **13,** 25–35
4. Lee, D. K., Cheng, R., Nguyen, T., Fan, T., Kariyawasam, A. P., Liu, Y., Osmond, D. H., George, S. R., and O'Dowd, B. F. (2000) *J. Neurochem.* **74,** 34–41
5. De Mota, N., Reaux-Le Goazigo, A., El Messari, S., Chartrel, N., Roesch, D., Dujardin, C., Kordon, C., Vaudry, H., Moos, F., and Llorens-Cortes, C. (2004) *Proc. Natl. Acad. Sci. U.S.A.* **101,** 10464–10469
6. Kawamata, Y., Habata, Y., Fukusumi, S., Hosoya, M., Fujii, R., Hinuma, S., Nishizawa, N., Kitada, C., Onda, H., Nishimura, O., and Fujino, M. (2001) *Biochim. Biophys. Acta* **1538,** 162–171
7. Medhurst, A. D., Jennings, C. A., Robbins, M. J., Davis, R. P., Ellis, C., Winborn, K. Y., Lawrie, K. W., Hervieu, G., Riley, G., Bolaky, J. E., Herrity, N. C., Murdock, P., and Darker, J. G. (2003) *J. Neurochem.* **84,** 1162–1172
8. Zhou, N., Fan, X., Mukhtar, M., Fang, J., Patel, C. A., DuBois, G. C., and Pomerantz, R. J. (2003) *Virology* **307,** 22–36
9. De Mota, N., Lenkei, Z., and Llorens-Cortès, C. (2000) *Neuroendocrinology* **72,** 400–407
10. Masri, B., Morin, N., Cornu, M., Knibiehler, B., and Audigier, Y. (2004) *FASEB J.* **18,** 1909–1911
11. El Messari, S., Iturrioz, X., Fassot, C., De Mota, N., Roesch, D., and Llorens-Cortes, C. (2004) *J. Neurochem.* **90,** 1290–1301
12. Reaux, A., De Mota, N., Skultetyova, I., Lenkei, Z., El Messari, S., Gallatz, K., Corvol, P., Palkovits, M., and Llorens-Cortès, C. (2001) *J. Neurochem.* **77,** 1085–1096
13. Evans, N. A., Groarke, D. A., Warrack, J., Greenwood, C. J., Dodgson, K., Milligan, G., and Wilson, S. (2001) *J. Neurochem.* **77,** 476–485
14. O'Carroll, A. M., Selby, T. L., Palkovits, M., and Lolait, S. J. (2000) *Biochim. Biophys. Acta* **21,** 72–80
15. Reaux, A., Gallatz, K., Palkovits, M., and Llorens-Cortes, C. (2002) *Neuroscience* **113,** 653–662
16. O'Carroll, A. M., and Lolait, S. J. (2003) *J. Neuroendocrinol.* **15,** 661–666
17. Reaux-Le Goazigo, A., Morinville, A., Burlet, A., Llorens-Cortes, C., and Beaudet, A. (2004) *Endocrinology* **145,** 4392–4400
18. Azizi, M., Iturrioz, X., Blanchard, A., Peyrard, S., De Mota, N., Chartrel, N., Vaudry, H., Corvol, P., and Llorens-Cortes, C. (2008) *J. Am. Soc. Nephrol.* **19,** 1015–1024
19. Japp, A. G., and Newby, D. E. (2008) *Biochem. Pharmacol.* **75,** 1882–1892
20. Tatemoto, K., Takayama, K., Zou, M. X., Kumaki, I., Zhang, W., Kumano, K., and Fujimiya, M. (2001) *Regul. Pept.* **99,** 87–92
21. Japp, A. G., Cruden, N. L., Amer, D. A., Li, V. K., Goudie, E. B., Johnston, N. R., Sharma, S., Neilson, I., Webb, D. J., Megson, I. L., Flapan, A. D., and Newby, D. E. (2008) *J. Am. Coll. Cardiol.* **52,** 908–913
22. Ishida, J., Hashimoto, T., Hashimoto, Y., Nishiwaki, S., Iguchi, T., Harada, S., Sugaya, T., Matsuzaki, H., Yamamoto, R., Shiota, N., Okunishi, H., Kihara, M., Umemura, S., Sugiyama, F., Yagami, K., Kasuya, Y., Mochizuki, N., and Fukamizu, A. (2004) *J. Biol. Chem.* **279,** 26274–26279
23. Lee, D. K., Saldivia, V. R., Nguyen, T., Cheng, R., George, S. R., and O'Dowd, B. F. (2005) *Endocrinology* **146,** 231–236
24. Ashley, E. A., Powers, J., Chen, M., Kundu, R., Finsterbach, T., Caffarelli, A., Deng, A., Eichhorn, J., Mahajan, R., Agrawal, R., Greve, J., Robbins, R., Patterson, A. J., Bernstein, D., and Quertermous, T. (2005) *Cardiovasc. Res.* **65,** 73–82
25. Berry, M. F., Pirolli, T. J., Jayasankar, V., Burdick, J., Morine, K. J., Gardner, T. J., and Woo, Y. J. (2004) *Circulation* **110,** Suppl. 1, II187–II193
26. Szokodi, I., Tavi, P., Földes, G., Voutilainen-Myllylä, S., Ilves, M., Tokola, H., Pikkarainen, S., Piuhola, J., Rysä, J., Tóth, M., and Ruskoaho, H. (2002) *Circ. Res.* **91,** 434–440
27. Kuba, K., Zhang, L., Imai, Y., Arab, S., Chen, M., Maekawa, Y., Leschnik, M., Leibbrandt, A., Markovic, M., Schwaighofer, J., Beetz, N., Musialek, R., Neely, G. G., Komnenovic, V., Kolm, U., Metzler, B., Ricci, R., Hara, H., Meixner, A., Nghiem, M., Chen, X., Dawood, F., Wong, K. M., Sarao, R., Cukerman, E., Kimura, A., Hein, L., Thalhammer, J., Liu, P. P., and Penninger, J. M. (2007) *Circ. Res.* **101,** e32–e42
28. Archer-Lahlou, E., Tikhonova, I., Escrieut, C., Dufresne, M., Seva, C., Pradayrol, L., Moroder, L., Maigret, B., and Fourmy, D. (2005) *J. Med. Chem.* **48,** 180–191
29. Hénin, J., Maigret, B., Tarek, M., Escrieut, C., Fourmy, D., and Chipot, C. (2006) *Biophys. J.* **90,** 1232–1240
30. Tikhonova, I. G., Marco, E., Lahlou-Archer, E., Langer, I., Foucaud, M., Maigret, B., and Fourmy, D. (2007) *Curr. Top. Med. Chem.* **7,** 1243–1247
31. Humphrey, W., Dalke, A., and Schulten, K. (1996) *J. Mol. Graph.* **14,** 33–38
32. Phillips, J. C., Braun, R., Wang, W., Gumbart, J., Tajkhorshid, E., Villa, E., Chipot, C., Skeel, R. D., Kalé, L., and Schulten, K. (2005) *J. Comput. Chem.* **26,** 1781–1802
33. Cai, W., Shao, X., and Maigret, B. (2002) *J. Mol. Graph. Model.* **20,** 313–328
34. Cai, W., Xu, J., Shao, X., Leroux, V., Beautrait, A., and Maigret, B. (2008) *J. Mol. Model* **14,** 393–401
35. Iturrioz, X., Alvear-Perez, R., De Mota, N., Franchet, C., Guillier, F., Leroux, V., Dabire, H., Le Jouan, M., Chabane, H., Gerbier, R., Bonnet, D., Berdeaux, A., Maigret, B., Galzi, J. L., Hibert, M., and Llorens-Cortes, C. (2010) *FASEB J.* **24,** 1506–1517
36. Lenkei, Z., Beaudet, A., Chartrel, N., De Mota, N., Irinopoulou, T., Braun, B., Vaudry, H., and Llorens-Cortes, C. (2000) *J. Histochem. Cytochem.* **48,** 1553–1564
37. Iturrioz, X., Vazeux, G., Célérier, J., Corvol, P., and Llorens-Cortès, C. (2000) *Biochemistry* **39,** 3061–3068
38. Drake, M. T., Violin, J. D., Whalen, E. J., Wisler, J. W., Shenoy, S. K., and Lefkowitz, R. J. (2008) *J. Biol. Chem.* **283,** 5669–5676
39. Galandrin, S., and Bouvier, M. (2006) *Mol. Pharmacol.* **70,** 1575–1584
40. Shukla, A. K., Violin, J. D., Whalen, E. J., Gesty-Palmer, D., Shenoy, S. K., and Lefkowitz, R. J. (2008) *Proc. Natl. Acad. Sci. U.S.A.* **105,** 9988–9993
41. Swaminath, G., Xiang, Y., Lee, T. W., Steenhuis, J., Parnot, C., and Kobilka, B. K. (2004) *J. Biol. Chem.* **279,** 686–691

42. Befort, K., Tabbara, L., Kling, D., Maigret, B., and Kieffer, B. L. (1996) *J. Biol. Chem.* **271,** 10161–10168
43. Govaerts, C., Bondue, A., Springael, J. Y., Olivella, M., Deupi, X., Le Poul, E., Wodak, S. J., Parmentier, M., Pardo, L., and Blanpain, C. (2003) *J. Biol. Chem.* **278,** 1892–1903
44. Madabushi, S., Gross, A. K., Philippi, A., Meng, E. C., Wensel, T. G., and Lichtarge, O. (2004) *J. Biol. Chem.* **279,** 8126–8132
45. Roth, B. L., Shoham, M., Choudhary, M. S., and Khan, N. (1997) *Mol. Pharmacol.* **52,** 259–266
46. Stitham, J., Stojanovic, A., Ross, L. A., Blount, A. C., Jr., and Hwa, J. (2004) *Biochemistry* **43,** 8974–8986
47. Chauvin, S., Hibert, M., Bérault, A., and Counis, R. (2001) *Biochem. Pharmacol.* **62,** 329–334
48. Rhee, M. H., Nevo, I., Bayewitch, M. L., Zagoory, O., and Vogel, Z. (2000) *J. Neurochem.* **75,** 2485–2491
49. Suzuki, T., Namba, K., Yamagishi, R., Kaneko, H., Haga, T., and Nakata, H. (2009) *J. Neurochem.* **110,** 1352–1362
50. Braden, M. R., Parrish, J. C., Naylor, J. C., and Nichols, D. E. (2006) *Mol. Pharmacol.* **70,** 1956–1964
51. Chen, S., Lin, F., Xu, M., and Graham, R. M. (2002) *Biochemistry* **41,** 588–596
52. Chen, S., Lin, F., Xu, M., Riek, R. P., Novotny, J., and Graham, R. M. (2002) *Biochemistry* **41,** 6045–6053
53. Pulakat, L., Mandavia, C. H., and Gavini, N. (2004) *Biochem. Biophys. Res. Commun.* **319,** 1138–1143
54. Hunter, C. A., Singh, J., and Thornton, J. M. (1991) *J. Mol. Biol.* **218,** 837–846
55. Thomas, A., Meurisse, R., and Brasseur, R. (2002) *Proteins* **48,** 635–644
56. Han, H. M., Shimuta, S. I., Kanashiro, C. A., Oliveira, L., Han, S. W., and Paiva, A. C. (1998) *Mol. Endocrinol.* **12,** 810–814
57. Wess, J., Nanavati, S., Vogel, Z., and Maggio, R. (1993) *EMBO J.* **12,** 331–338
58. Chen, M. M., Ashley, E. A., Deng, D. X., Tsalenko, A., Deng, A., Tabibiazar, R., Ben-Dor, A., Fenster, B., Yang, E., King, J. Y., Fowler, M., Robbins, R., Johnson, F. L., Bruhn, L., McDonagh, T., Dargie, H., Yakhini, Z., Tsao, P. S., and Quertermous, T. (2003) *Circulation* **108,** 1432–1439
59. Chini, B., Mouillac, B., Balestre, M. N., Trumpp-Kallmeyer, S., Hoflack, J., Hibert, M., Andriolo, M., Pupier, S., Jard, S., and Barberis, C. (1996) *FEBS Lett.* **397,** 201–206
60. Escrieut, C., Gigoux, V., Archer, E., Verrier, S., Maigret, B., Behrendt, R., Moroder, L., Bignon, E., Silvente-Poirot, S., Pradayrol, L., and Fourmy, D. (2002) *J. Biol. Chem.* **277,** 7546–7555
61. Yamano, Y., Ohyama, K., Kikyo, M., Sano, T., Nakagomi, Y., Inoue, Y., Nakamura, N., Morishima, I., Guo, D. F., and Hamakubo, T. (1995) *J. Biol. Chem.* **270,** 14024–14030